CIRP Annals - Manufacturing Technology 67 (2018) 405–408

Contents lists available at ScienceDirect

CIRP Annals - Manufacturing Technology

journal homepage: http://ees.elsevier.com/cirp/default.asp

An active non-contact journal bearing with bi-directional driving capability utilizing coupled resonant mode

Ping Guo *, Han Gao

Department of Mechanical and Automation Engineering, The Chinese University of Hong Kong, Hong Kong, China

Submitted by Ajay P. Malshe (1), Mechanical Engineering, University of Arkansas, Fayetteville, AR, USA.

ARTICLE INFO

Article history:
Available online 13 April 2018

Keywords:
Ultrasonic
Bearing
Acoustic levitation

ABSTRACT

Non-contact journal bearings are conventionally based on pressurized air or magnetic levitation. This paper reports on a new design of an active non-contact journal bearing with bi-direction driving capabilities. It combines the functions of an axis positioner, non-contact journal bearing, and rotary motor utilizing coupled vibration modes. The shaft levitation is achieved by creating a stable air film using near-field acoustic force; while the non-contact rotation is realized by controlling the pressure distribution within the air film using coupled resonant mode. The essential design methodology and theoretical principles are presented along with the performance evaluation of the functional prototypes.

1. Introduction

Journal bearings are utilized in all kinds of transmission mechanisms, such as measurement instruments, semiconductor-manufacturing, and precision machine tools. The friction reduction between contact surfaces plays a crucial role in their performance because friction force leads to undesirable wear, heat generation, low efficiency, short life spans, and low reliability. In machine tools, aerostatic, aerodynamic, and electromagnetic bearings are predominant for ultra-precision applications, but they are still suffering from high-cost, unpleasant noise, complex system design, and limitation in miniaturization [1].

An alternative solution for non-contact bearing design has been investigated based on near-field acoustic levitation. When a flat surface is placed close to an ultrasonically oscillating ground surface, levitation force is observed due to the nonsymmetric cyclic pressure developed in the thin air film between the two surfaces [2,3]. The phenomenon can be intuitively explained by the fact that air is a viscous medium, which cannot be squeezed out from the side openings instantaneously giving rise to the non-zero time-averaged levitation force. It is sometimes also referred to as the squeeze film levitation, since the levitation force becomes significant only when the air film thickness is in the range of several to tens of micrometers.

Non-contact linear acoustic bearings were developed by utilizing high frequency vibration of the cartridge [4] and the linear guide rail [5]. A traveling wave could be generated along the guide rail to introduce acoustic streaming within the air gap for one-dimensional non-contact transportation [6]. Alternatively, the levitated object could be used as the vibration source to generate near-field acoustic pressure to act as a self-floating or self-running actuator [7]. The application of near-field acoustic levitation in a conformal contact led to the development of non-contact journal bearings and rotary motors. The resonant vibration of the structure was utilized to create a stable air film, including designs based on normal vibration of Langevin-type transducers [8,9] and flexural modes of tubular sleeve structures [10]. Similar to the design of acoustic linear guide rails, traveling waves are utilized in an annular shaped stator to produce a pressure gradient in the circumferential direction for non-contact drive of the rotor [11].

In this paper, a novel compact journal bearing design is proposed which combines the functions of an axis positioner, non-contact bearing, and rotary motor by utilizing the coupled resonant modes of a single structure unit. It enables the mode switch between pure levitation (non-contact bearing) and rotation (non-contact motor), as well as the bi-directional rotational speed control by adjusting the phase angle of input excitations. The radial position of the shaft can also be actively controlled in submicron scale. In addition, the proposed design is unique in terms of its driving mechanism. The rotational driving force is provided by the projection of the normal levitation force in the tangential direction rather than the pressure gradient induced by a traveling wave, which significantly increases its power efficiency.

The design principle is first introduced in this paper, followed by analytical modeling of the levitation and driving mechanisms. Numerical simulation results of the driving force and pressure distribution are obtained based on the actual mode shapes extracted from finite element analysis. A single driving unit is built and evaluated to verify our design principle and analytical model. In the end, an advanced prototype with six driving units is demonstrated for its two-dimensional radial position control and driving capabilities.

* Corresponding author.
E-mail address: pguo@mae.cuhk.edu.hk (P. Guo).

https://doi.org/10.1016/j.cirp.2018.03.008
0007-8506/

2. Operation principle and dynamic modeling

The design of the journal bearing is illustrated in Fig. 1(a). It consists of a horn structure with a concave end surface, two stacked piezoelectric rings, and a preloading bolt. The whole structure is carefully designed to have its first longitudinal mode and second bending mode located very closely in the frequency space, as shown in Fig. 1(c). The piezoelectric rings, which are sandwiched between the horn and base structures, have two

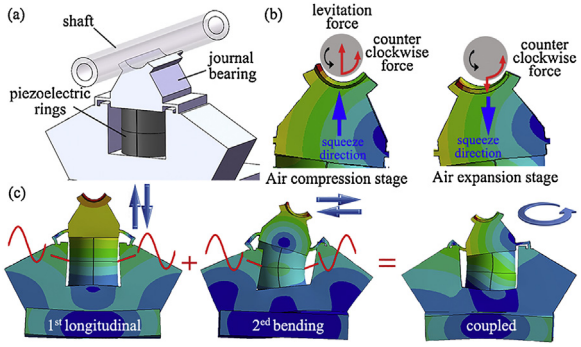

Fig. 1. (a) Design of a single driving unit; (b) operation principle for shaft levitation and rotation; and (c) coupled mode shapes.

isolated half-moon electrodes that can be energized individually.

When the two excitation signals are in-phase, the longitudinal mode will be excited resulting in pure levitation of the shaft due to the uniform squeezing of the air film. When the two excitation signals are in antiphase, the bending mode is excited resulting in pure levitation because of the symmetric squeezing motion over a vibration cycle. When the phase angle is set between 0 and 180°, the superposition of the longitudinal and bending modes will result in elliptical vibration of the structure. This will provide both vertical levitation and lateral driving force in the tilt direction of the elliptical vibration trajectory. The shaft rotation direction and speed can be controlled by adjusting the relative phase angle between −180° to 180°, which in essence adjusts the relative mode amplitudes of the longitudinal and bending modes.

The mechanism of non-contact rotation can be explained by the schematics shown in Fig. 1(b). Unlike previous designs utilizing a traveling wave and viscous shear force, the rotational driving force is mainly contributed by the tangential component of the levitation pressure. During the compression stage of the air film, due to the slope angle of the bearing upper surface, the net reaction force from the air produces a circumferential force acting in the counter clockwise direction of the shaft. During the release stage, both the bearing surface slope angle and the pressure force change the direction, so the net reaction force still produces a counter clockwise torque on the shaft. For both the compression and expansion stages, the reaction force applied on the shaft has a circumferential component in the same direction.

In order to theoretically understand the levitation and driving mechanisms of the proposed design, a 2D analytical model is set up as shown in Fig. 2. The annular-shaped domain is the air film in question, which is bounded by the bearing and shaft surfaces. A polar coordinate system is established by unfolding the air film in the angular direction. The upper boundary is the shaft surface, which is assumed to be fixed (for pure levitation) or moving at a linear velocity of v_θ (for non-contact driving). The two side boundaries are open to atmospheric pressure. The lower boundary

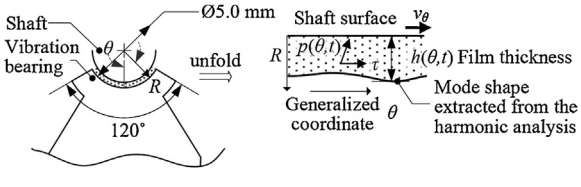

Fig. 2. Model setup for the generalized 1D Reynolds equation.

is defined by the mode shapes of the tuning-fork-shaped driving plate. The mode shapes, including the amplitude and phase information, are extracted from the simulation results of harmonic analysis for the longitudinal, bending and coupled vibration modes. They are then converted to the polar coordinates to derive the dynamic film thickness distribution.

The air film thickness is assumed to be much smaller than the lateral characteristic length of the domain, so the pressure variation across the film thickness is negligible. If we further ignore the inertial effect of air and assume a Newtonian compressible fluid, the time-varying pressure distribution in the domain can be described by a modified 1D Reynolds equation [12]. The final dimensionless equation expressed in the polar coordinate system becomes:

$$\frac{\partial}{\partial\theta}\left(H^3P\frac{\partial P}{\partial\theta}-\Lambda PH\right)-\sigma P\frac{\partial H}{\partial T}=\sigma H\frac{\partial P}{\partial T} \tag{1}$$

where $H(\theta,t)$, T, θ are the dimensionless film thickness, time and generalized coordinate, respectively. $P(\theta,t)$ is the dimensionless pressure, defined as the ratio of absolute pressure to atmospheric pressure. Λ and σ are the bearing and squeeze numbers [12].

The input function to the governing equation is the dimensionless film thickness, which is given by

$$H(\theta,t)=h(\theta,t)/h_0=1-\delta A_r(\theta)\sin(\omega t+\phi_r(\theta)) \tag{2}$$

where $A_r(\theta)$ and $\phi_r(\theta)$ are the normalized mode amplitude and phase extracted from the harmonic analysis. δ stands for the compression ratio, indicating the ratio of the mean vibration amplitude to mean clearance.

The dimensionless levitation pressure is then calculated by averaging the pressure in the temporal and spatial domains, considering the generalized coordinates, as:

$$F_l=\frac{3}{4\pi^2}\int_0^{2\pi}\int_{-\pi/3}^{\pi/3}(P-1)\cos\theta\,d\theta dT \tag{3}$$

The driving force in the circumferential direction is contributed by two parts. One is the viscous force due to the pressure gradient in the tangential direction. The other one comes from the projection of the reaction pressure in the tangential direction due to the tiling angle of the driving plate, which can be approximated by the partial derivative of the film thickness with respect to the generalized coordinate. The dimensionless driving force can be calculated by combining the shear stress and the projection of levitation force in the tangential direction. The expression is given by averaging the result over the length and one period:

$$F_d=\frac{3}{4\pi^2}\int_0^{2\pi}\int_{-\pi/3}^{\pi/3}\left[\frac{1}{2}\frac{\partial P}{\partial\theta}(P-1)+\frac{dH}{d\theta}\right]d\theta dT \tag{4}$$

The parameter settings for the numerical simulation are summarized in Table 1. Three representative cases have been calculated corresponding to the pure longitudinal, pure bending, and coupled vibration at a compression ratio of 0.35. The spatial distribution (X axis) and time evolution (Y axis) of the dimensionless pressure, $P(\theta,t)$, and air film thickness, $H(\theta,t)$, are plotted in Fig. 3(a–d) respectively. The pressure difference in a period is larger than zero due to the squeeze film levitation effect, which provides a positive levitation force. The time-averaged pressure distribution is then illustrated and compared in Fig. 4. For the longitudinal

Table 1
Parameter settings for the numerical simulation.

	Longitudinal mode	Bending mode	Coupled mode
Common properties	Mean clearance h_0 = 15 μm Arc length L = 5.2 mm Compression ratio δ = 0.35	Viscosity μ = 1.81×10^{-5}Pa·s Frequency f = 42.7 kHz Squeeze number σ = 78.5	
Bearing number	Λ = 0 v_θ = 0	Λ = 0 v_θ = 0	Λ = 0.0065 v_θ = 0.3 m/s
Phase angle	0°	180°	90°

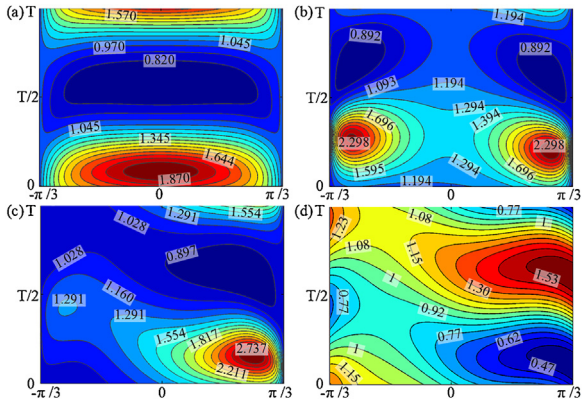

Fig. 3. Pressure distribution for (a) longitudinal, (b) bending, and (c) coupled modes; and (d) film thickness distribution for the coupled mode.

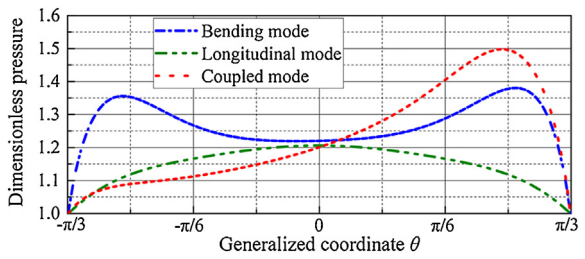

Fig. 4. Time-averaged pressure distribution for the longitudinal, bending and coupled modes.

mode, the time-averaged pressure is at its maximum at the center and gradually drops to atmospheric pressure at the two open ends. For the bending mode, the pressure distribution is symmetric with respect to the center position, resulting in pure levitation only.

For the coupled resonant mode, the pressure distribution is not symmetric with respect to the spatial or temporal axes. The pressure gradient leads to the viscous driving force, which is much smaller than the tangential component of the acoustic pressure (more than one order of magnitude). The local curvature, $\partial H/\partial\theta$, and the pressure both flip their sign between the compression and release stages, so their product will always contribute positively to the driving force. For the three representative simulation cases, the calculated dimensionless levitation pressure was 0.13, 0.22, and 0.19 for the longitudinal, bending and coupled modes. The driving force was determined to be 0.055 for the coupled mode.

3. Single unit prototype and experimental verification

A single unit prototype was built based on the optimized geometry from finite element simulation. The prototype along with the measurement setup is shown in Fig. 5. The excitation signals were generated using a dual-channel function generator (*TTi* TG5012A) and amplified through a piezo amplifier (*Trek* PZD 350A). The shaft levitation height was measured using a capacitance probe (*MicroSense* 5504), which has a measurement range of 100 μm and a bandwidth of 100 kHz. The rotation speed of the shaft was measured using a laser speed gauge (*Suwei* SW826). The measurement data were recorded

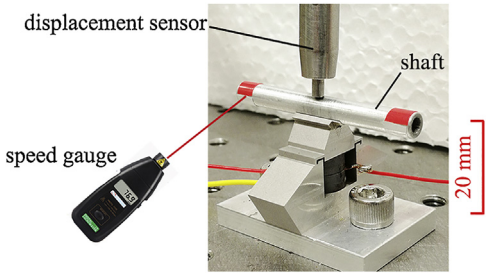

Fig. 5. Prototype design with the measurement setup.

using an oscilloscope (*Tektronix* MSO2004B). The aluminum hollow shaft had an outer diameter of 5 mm and an inner diameter of 3 mm. The mass was 1.5 g; and the moment of inertia was 27.2 g mm^2.

The two halves of the piezoelectric rings were individually excited with two sinusoidal signals of the same frequency and amplitude but with a phase difference between the two. The longitudinal mode was excited by setting the phase angle to 0, while the bending mode was excited by setting the phase angle to 180°. The influences of driving frequency and mode shape on the levitation height were evaluated using a sine sweep test as shown in Fig. 6. The resonant frequencies of the longitudinal and bending modes were identified to be at 47.9 kHz and 43.8 kHz respectively. The coupled operating frequency was chosen between the two modes. The best performance in terms of symmetric bidirectional rotational speed and stability was experimentally determined at 47.2 kHz.

The experimental results of the levitation and rotational driving tests are summarized in Fig. 7. When the phase angle was set to

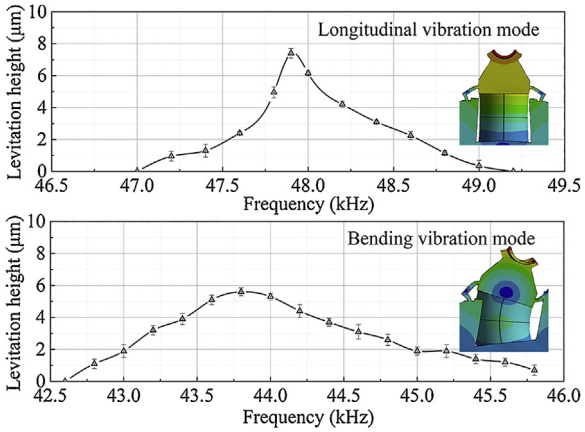

Fig. 6. Relationship between the frequency and levitation height.

0 and the excitation frequency was 47.9 kHz, the bearing worked at the longitudinal mode. Pure levitation of the shaft without rotation was observed, which is predicted by our numerical model. The levitation height was detected when the excitation voltage amplitude exceeded 100 V. The levitation height increased rapidly to 7.5 μm with the increase in the voltage amplitude from 100 V to 150 V, then followed a linear relationship with the input voltage. The maximal levitation height exceeded 15.6 μm at an input voltage amplitude of 300 V. Similarly, when operated at the pure bending mode with a 180° phase angle and a driving frequency of 43.8 kHz, pure levitation of the shaft was observed as predicted. The levitation height increased linearly with the input voltage amplitude from 50 V and reached a peak value of 13.4 μm at 300 V.

The non-contact shaft rotation can be achieved and controlled by exciting the structure at a frequency between the two modes and adjusting the input phase angle or input voltage amplitude. The bearing was excited at 47.2 kHz with a voltage amplitude of 300 V, while the phase angle was adjusted from −180° to +180°. The relationship between the rotation direction as well as speed and the input phase angle is plotted in Fig. 8. The bearing demonstrated identical performance when rotated in the clock-

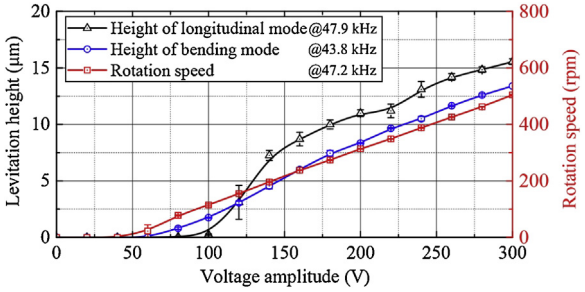

Fig. 7. Performance evaluation of levitation height and rotation speed.

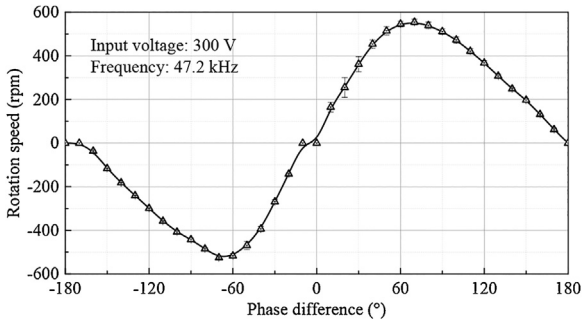

Fig. 8. The relationship between rotation speed and phase angle.

wise and counter clockwise directions. The rotation speed reached a peak value of ±555 rpm at a phase angle of 70°. The bearing could be switched to a pure levitation state by setting the phase angle to 0° or 180°. When the phase angle was fixed at 70°, the relationship between voltage amplitude and rotation speed was explored. The result shows a good linearity between the input voltage and rotation speed as illustrated in Fig. 7.

4. An active bearing design with axis position control

Based on the design principle proposed in this paper, an advanced functional prototype with six driving units was fabricated for two-dimensional radial position control. The 3D model and functional prototype are shown in Fig. 9. The main body of a U-shaped bearing frame was fabricated from a single aluminum alloy workpiece using electrical discharge machining (EDM) to ensure the coaxiality between the two sets of driving units. On each side, three identical driving units are placed 120° apart. Each driving unit functions similarly as the single unit described in the previous sections. The overall operating frequency

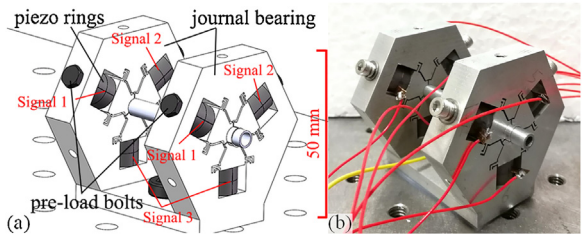

Fig. 9. Design of the active non-contact journal bearing with six driving units: (a) 3D model and (b) functional prototype.

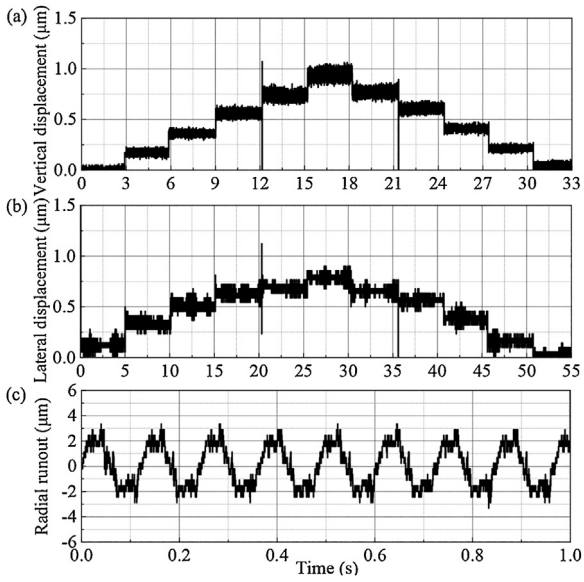

Fig. 10. Active axis position control in the (a) vertical and (b) lateral directions; and (c) shaft runout during rotation.

of this design would be higher than that in a single unit due to the increased stiffness from the unibody design.

In additional to the levitation and rotation control, the radial position control capability is demonstrated. The driving units were grouped by their angular position and controlled by the signals #1–#3, as shown in Fig. 9. In the vertical direction, the shaft position could be controlled in a range of 18.3 μm, when the signals #1 and #2 were simultaneously varied from 100 V to 350 V. The minimal stable increment could reach 200 nm when the voltage increment was 5 V, as shown in Fig. 10(a). In the lateral direction, the radial position could be controlled in a range of 2.1 μm, when we adjusted the amplitudes of signals #1 and #2 in the opposite direction. The minimal stable increment could also reach 200 nm when the voltage increment was 10 V, as shown in Fig. 10(b). Finally, the radial runout was measured at a rotation speed of 512 rpm, when the driving frequency was 64.9 kHz with a 75° phase shift angle. The total indicator runout was within 6 μm as indicated in Fig. 10(c), which is a combination from the shaft form inaccuracy and spindle runout.

5. Conclusions

An active non-contact journal bearing is proposed with the bi-directional driving capability utilizing coupled resonant vibration. The design utilizes a single structure and its coupled resonant modes to achieve near-field acoustic levitation and non-contact driving. The driving mechanism is unique that it relies on the tangential projection of the normal levitation pressure rather than the viscous force, which significantly improves its energy efficiency. The rotation speed can be easily controlled within ±555 rpm by adjusting the input phase angle. The pure levitation state can be achieved by setting the phase angle to 0 or 180°. An advanced prototype with six driving units has been demonstrated for two-dimensional radial position control with a minimal increment step of 200 nm.

Acknowledgements

This work has been supported by the Shun Hing Institute of Advanced Engineering, CUHK, #RNE-p4-17; and the Research Grants Council of Hong Kong, #ECS 24201816. The authors would like to thank Mr. Derik Epperson for his constructive comments.

References

[1] Abele E, Altintas Y, Brecher C (2010) Machine Tool Spindle Units. *CIRP Annals* 59 (2):781–802.
[2] Hashimoto Y, Koike Y, Ueha S (1995) Acoustic Levitation of Planar Objects Using a Longitudinal Vibration Mode. *Journal of the Acoustical Society of Japan (E)* 16(3):189–192.
[3] Minikes A, Bucher I, Haber S (2004) Levitation Force Induced by Pressure Radiation in Gas Squeeze Films. *The Journal of the Acoustical Society of America* 116(1):217–226.
[4] Stolarski T, Chai W (2006) Self-levitating Sliding Air Contact. *International Journal of Mechanical Sciences* 48(6):601–620.
[5] Ide T, Friend J, Nakamura K, Ueha S (2007) A Non-contact Linear Bearing and Actuator via Ultrasonic Levitation. *Sensors and Actuators A: Physical* 135 (2):740–747.
[6] Hashimoto Y, Koike Y, Ueha S (1998) Transporting Objects without Contact Using Flexural Traveling Waves. *The Journal of the Acoustical Society of America* 103(6):3230–3233.
[7] Chen K, Gao S, Pan Y, Guo P (2016) Self-running and Self-floating Two-dimensional Actuator Using Near-field Acoustic Levitation. *Applied Physics Letters* 109(12):123503.
[8] Li H, Quan Q, Deng Z, Hua Y, Wang Y, Bai D (2016) A Novel Noncontact Ultrasonic Levitating Bearing Excited by Piezoelectric Ceramics. *Applied Sciences* 6(10):280.
[9] Zhao S, Mojrzisch S, Wallaschek J (2013) An Ultrasonic Levitation Journal Bearing Able to Control Spindle Center Position. *Mechanical Systems and Signal Processing* 36(1):168–181.
[10] Wang C, Au YJ (2012) Levitation Characteristics of a Squeeze-film Air Journal Bearing at its Normal Modes. *The International Journal of Advanced Manufacturing Technology* 60(1-4):1––10.
[11] Yamazaki T, Hu J, Nakamura K, Ueha S (1996) Trial Construction of a Noncontact Ultrasonic Motor with an Ultrasonically Levitated Rotor. *Japanese Journal of Applied Physics* 35(5S):3286.
[12] Langlois W (1962) Isothermal Squeeze Films. *Quarterly of Applied Mathematics* 20(2):131–150.